Solution growth of Ta-doped hematite nanorods for efficient photoelectrochemical water Splitting: a tradeoff between electronic structure and nanostructure evolution

*Yanming Fu,[a] Chung-Li Dong,[b] Zhaohui Zhou,[a] Wan-Yi Lee,[c] Jie Chen,[a] Penghui Guo,[a] Liang Zhao,[a] and Shaohua Shen[a,]**

[a] International Research Center for Renewable Energy, State Key Laboratory of Multiphase Flow in Power Engineering, Xi'an Jiaotong University, Shaanxi 710049, China.

[b] Department of Physics, Tamkang University, 151 Yingzhuan Rd., Tamsui, New Taipei 25137, Taiwan.

[c] National Synchrotron Radiation Research Center, 101 Hsin-Ann Road, Hsinchu Science Park, Hsinchu 30076, Taiwan.

Experimental

Fabrication of Ta-doped α-Fe_2O_3 films

The Ta-doped α-Fe_2O_3 films were grown onto fluorine-doped tin dioxide (FTO, Nippon Sheet Glass) coated glass substrates *via* the aqueous solution growth method described by Vayssieres, with minor modification. FTO glasses (2.5 cm × 4 cm) were sequentially sonicated in acetone, alcohol and deionized water for 10 min each. Then, two back-to-back FTO substrates were inserted into a cap-sealed glass bottle containing an 20 mL of aqueous solution of 0.15 M ferric

chloride ($FeCl_3$•$6H_2O$, analytically pure), 1 M sodium nitrate ($NaNO_3$, analytically pure), 50 μL of concentrated hydrochloric acid (HCl, 37.5 wt%) and desired amount of $TaCl_5$ as Ta doping precursor. The glass bottle was transferred into a regular oven and heated at 100 °C for 24 hours. After naturally cooled to room temperature, the yellowish films (akaganite, β-FeOOH nanorod bundles) formed on FTO substrates were thoroughly rinsed by deionized water and dried at room temperature, then annealed at 750 ºC for 30 min with ramping rate of 25 ºC/min. The obtained Ta-doped α-Fe_2O_3 films were denoted as TaFe-x (x =0, 2, 5, 10, 20, 50, 100), where x represents the weight (mg) of $TaCl_5$ added in the precursor solution.

Characterization

The film morphology was studied using a JEOL JSM-7800F field emission scanning electron microscope (FE-SEM) and a FEI Tecnai G2 F30 transmission electron micro-scope (TEM) with the accelerating voltage 300 kV. X-ray diffraction (XRD) measurements were carried out with an X-ray diffractometer (PANalytical) with Cu Kα irradiation (λ = 15.4184 nm). Raman scattering was performed on a Jobin Yvon LabRAM HR spectrometer using 514.5 nm irradiation from an argon ion laser at 20 mW. Spectral transmittance measurements were taken on the UV-visible spectrophotometer (Hitachi U-4100 UV–vis–near-IR). X-ray photoelectron spectroscopy (XPS) measurements were conducted to analyze the element compositions and states on a Kratos spectrometer (AXIS Ultra DLD) with monochromatic Al Kα radiation ($h\nu$ = 1486.69 eV) and with a concentric hemispherical analyzer. The synchrotron X-ray spectroscopy measurements at O *K*-edge and Fe *L*-edge were performed at BL20A at the National Synchrotron Radiation Research Center (NSRRC), Taiwan.

Photoelectrochemical measurements

Photocurrent measurements was carried out in a conventional three electrode cell in which α-Fe_2O_3 film was used as working electrode, platinum plate as counter electrode and Ag/AgCl (silver-silver chloride electrode) as reference electrode, respectively. An aqueous solution of 0.5 M Na_2SO_4 was used as electrolyte (pH = 6.5). A 300 W Xe lamp was used as the solar irradiated simulator with light intensity set at 100 $mW \cdot cm^{-2}$ through an AM 1.5G filter. N_2 gas was continuously bubbled in solution before and during all these electrochemical experiments to suppress the reduction of O_2 at the counter electrode by removing the dissolved O_2 in the solution. Incident photon-to-current conversion efficiency (IPCE) measurements were performed using a 300 W Xe lamp integrated with a computer-controlled monochromator, a photo chopper (PARC), and a lock-in amplifier used for photocurrent detection. IPCE measurements were also performed in the solution of 0.5 M Na_2SO_4 as electrolyte, and the applied potential was controlled at 1.0 V *vs.* Ag/AgCl reference electrode. Mott-Schottky (M-S) measurements were performed at 1 kHz frequency in 0.1 M NaOH electrolyte solution with the same three electrode configuration. The carrier density and flat-band potential could be obtained *via* the M-S equation: $1/C^2 = (2/e_0\varepsilon\varepsilon_0)[(V-V_{fb}) - kT/\varepsilon_0]$. According to the equation, the slope of the plots has a relationship with the carrier density: $N_d = (2/e_0\varepsilon\varepsilon_0)[d(1/C^2)/dV]^{-1}$, where N_d is the carrier density, V_{fb} is the flat-band potential, e_0 is the electron charge, ε is the relative dielectric constant of α-Fe_2O_3 (ε = 80), ε_0 is the permittivity of vacuum.[1,2]

Electronic structure calculations

The electronic structure calculations for Ta-doped α-Fe_2O_3 were performed within the framework of spin-polarized density functional theory with the on-site Coulomb correction (DFT+U) as implemented in the VASP code.[3,4] The exchange-correlation functional was treated within the

generalized gradient approximation (GGA) with the formalism of Perdew-Burke-Ernzerhofer (PBE).[5] The strongly correlated electronic nature in α-Fe_2O_3 was treated by the on-site Coulomb correction (U = 5 eV and J = 1 eV) [6] on Fe 3d electrons, while no Coulomb correction was introduced on the Ta atom. Projector augmented wave (PAW) potential [7] was employed to describe the electron-ion interaction. The plane-wave basis set with a 400 eV energy cutoff was used to expand the electronic wave function. The crystallographic unit cell was a hexagonal corundum structure with 18 O and 12 Fe atoms. The computational model for Ta-doped α-Fe_2O_3 was simulated by a Ta atom substituting for a Fe atom in the lattice site, and the Γ-centered k-point grid of 8×8×4 was adopted to sample the corresponding Brillouin zone. The valence electrons of O, Fe and Ta atoms were chosen as $2s^2 2p^4$, $3d^6 4s^2$ and $5p^6 6s^2 5d^3$, respectively, in the current calculation.

As shown in Figure S1, all the Ta-doped films display diffraction peaks well indexed to the α-Fe_2O_3 crystalline phase (JCPDS 33-0664), and no additional peaks assigned to impurity appear. However, diffraction peaks in the doped films with relatively high Ta doping concentration (TaFe-50 and TaFe-100) are very different from those of the other samples. By carefully checking the positions of these diffraction peaks, one can find that in the low concentration doping films (TaFe-x, x = 2, 5, 10, 20) XRD patterns are very similar to the undoped α-Fe_2O_3 film, with peaks exactly assigned to the (110), (113), (024), (214) and (300) planes of hematite crystalline, and the (110) reflection was the strongest, indicating the [110]-oriented growth of the α-Fe_2O_3 nanorod nanostructure. In comparison, in the high concentration doping films (TaFe-50 and TaFe-100), the (110), (113), (024), (214) and (300) peaks became very weak and even disappeared while some new diffraction peaks assigned to the (104), (116), (018) and (1010) planes turned up. It's hard to find any peak attributed to Ta metal oxides, due to the successful doping of Ta into α-Fe_2O_3 or the Ta contents below the XRD detection limitation.

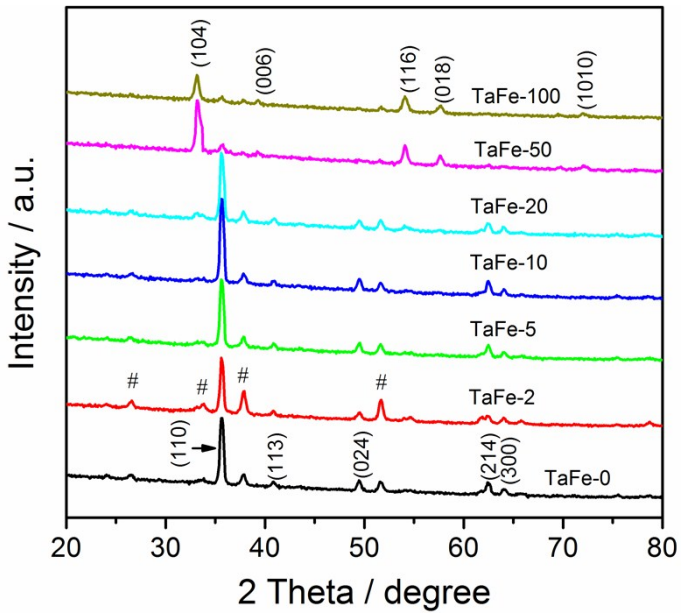

Figure S1. XRD patterns of undoped and Ta-doped α-Fe_2O_3 samples. Peaks from the FTO substrate are indicated by pound sign (#).

Crystal micro-structures of the undoped and Ta-doped α-Fe_2O_3 nanorod films were further detected by Raman spectra as shown in Figure S2A. The Raman peaks of undoped α-Fe_2O_3 nanorod film (TaFe-0) could be ascribed to the hematite crystalline phase. However, with the increase of Ta dopant contents, an additional weak peak at about 657 cm^{-1} gradually appeared for those Ta-doped α-Fe_2O_3 films, which should be assigned to the disorder phase induced by Ta doping. Such disorder has been frequently observed in the Raman spectra of doped α-Fe_2O_3 films [8] and also evidenced in HRTEM images in previous section. In addition, for the TaFe-50 and TaFe-100 films, a new peak at about 970 cm^{-1} appeared, which might be assigned to the characteristic Raman band of pure Ta_2O_5 by comparing with the Raman spectrum of Ta_2O_5 powder (Figure S2B). In short, the peak at 657 cm^{-1} supportively indicates that Ta ions were successfully introduced into the lattice of α-Fe_2O_3, while the peak at 970 cm^{-1} means superfluous Ta dopants could result in the emergence of Ta_2O_5 species in α-Fe_2O_3.

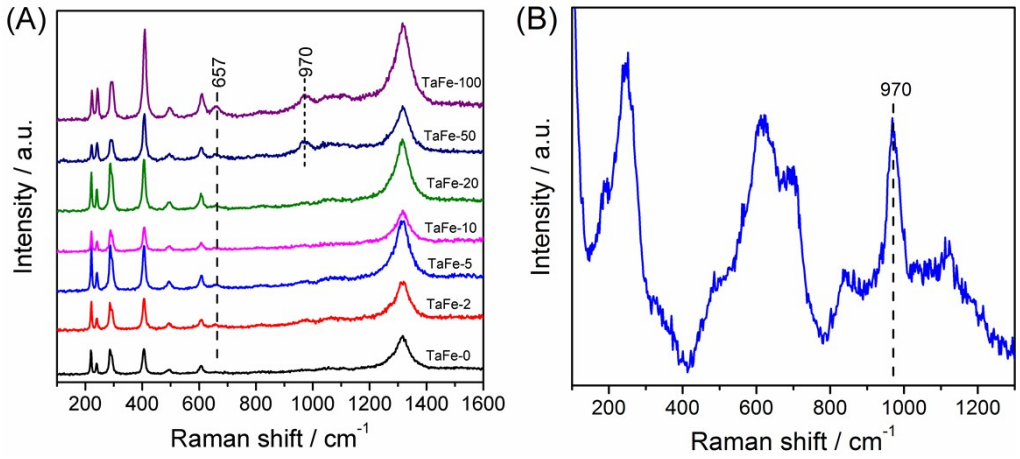

Figure S2. Raman spectra of (A) undoped and Ta-doped α-Fe_2O_3 films, and (B) pure Ta_2O_5 powder as reference.

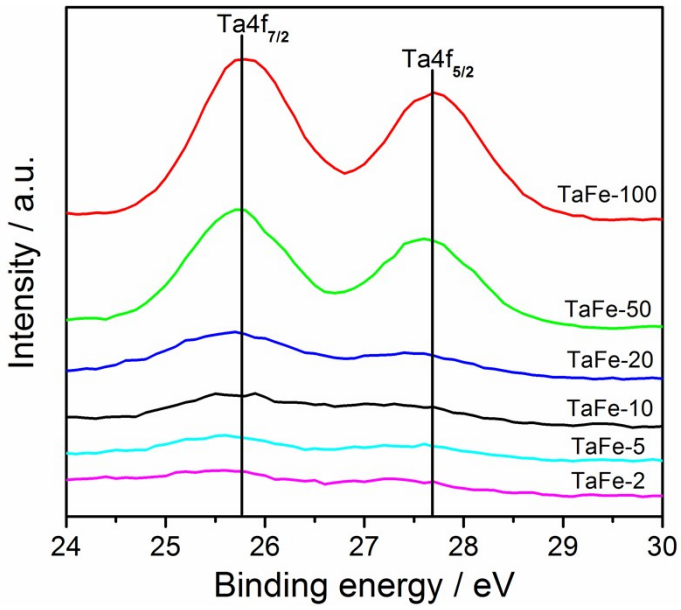

Figure S3. Ta4f XPS spectra of Ta-doped α-Fe_2O_3 films.

References

1. R. H. Goncalves, B. H. R. Lima and E. R. Leite, *J. Am. Chem. Soc.*, 2011, **133**, 6012–6019.

2. H. Tang, W.-J. Yin, M. A. Matin, H. Wang, T. Deutsch, M. M. Al-Jassim, J. A. Turner and Y. Yan, *J. Appl. Phys.*, 2012, **111**, 073502.

3. G. Kresse and J. Furthmuller, *Phys. Rev. B: Condens. Matter*, 1996, **54**, 11169–11186.

4. G. Kresse and J. Furthmuller, *Comput. Mater. Sci.*, 1996, **6**, 15–50.

5. J. P. Perdew, K. Burke and M. Ernzerhof, *Phys. Rev. Lett.*, 1996, **77**, 3865–3868.

6. A. I. Liechtenstein, V. I. Anisimov and J. Zaanen, *Phys. Rev. B: Condens. Matter*, 1995, **52**, R5467–R5470.

7. G. Kresse and D. Joubert, *Phys. Rev. B: Condens. Matter Mater. Phys.*, 1999, **59**, 1758–1775.

8. Y. S. Hu, A. Kleiman-Shwarsctein, A. J. Forman, D. Hazen, J. N. Park and E. W. McFarland, *Chem. Mater.*, 2008, **20**, 3803–3805.